Hindawi
Mathematical Problems in Engineering
Volume 2022, Article ID 8264359, 17 pages
https://doi.org/10.1155/2022/8264359

Research Article

Multisensor and Multitarget Tracking Based on Generalized Covariance Intersection Rule

Kuiwu Wang,[1,2] **Qin Zhang**,[1] **and Xiaolong Hu**[1]

[1]*School of Air Defense and Missile Defense, Air Force Engineering University, Xi'an 710051, China*
[2]*Graduate School of Air Force Engineering University, Xi'an 710051, China*

Correspondence should be addressed to Kuiwu Wang; wkw19971997@163.com

Received 21 March 2022; Revised 9 July 2022; Accepted 16 July 2022; Published 18 August 2022

Academic Editor: Ahmed Zeeshan

Distributed multitarget tracking (MTT) is suitable for sensors with limited field of view (FoV). Generalized covariance intersection (GCI) fusion is used to solve the MTT problem based on label probability hypothesis density (PHD) filtering in this paper. Because the traditional GCI fusion only has good fusion performance for the targets in the intersection of each sensor's FoV, and the targets outside the intersection range would be lost, this paper redivides the Gaussian components according to the FoV and distinguishes the Gaussian components of the targets inside and outside the intersection. GCI fusion is sensitive to label inconsistency between different sensors. For label fusion in the intersection region, the best match of labels is found by minimizing label inconsistency index, and then GCI fusion is performed. Finally, the feasibility and effectiveness of the proposed fusion method are verified by simulation, and its robustness is proved. The proposed method is obviously superior to local sensor and traditional GCI algorithm.

1. Introduction

MTT is a process of assigning the measurements to the targets, filtering them, and managing the tracks of multiple targets according to the time step [1, 2]. Traditional tracking algorithms, such as probabilistic data association (PDA), multiple hypothesis tracking (MHT), and others [3–6], transform the multitarget problem into a parallel single-target tracking problem by allocation of measurements. The core of its processing method is data correlation, but when there are many targets and a large number of false alarm clutter, correlation will bring combination explosion and make the calculation amount increase exponentially. Correlation error and state estimation error are coupled and influence each other, which results in large estimation error. The random finite set (RFS) provides a unified and clear framework for MTT. The first-order moment realization, that is, PHD filtering [7], avoids the complex data association problem in the process of state estimation, which can concentrate resources on tracking problems, and has good potential in solving target tracking problems under the conditions of insufficient prior knowledge and unknown number of targets. At present, it has been widely used in radar target tracking [8–10], computer vision [11], real-time positioning and map building [12], and group target tracking [13]. Among them, Gaussian mixture (GM) and sequential Monte Carlo (SMC) are two important methods of PHD operation, which are called GM-PHD [14] and SMC-PHD [15], respectively.

PHD filter has rigorous mathematical theoretical basis and can realize joint detection and tracking of targets. The structure is complete and clear, and the amount of calculation is small. However, PHD filter cannot identify the tracks of different targets in the tracking process. With the increase of targets or the approach of distances, the wrong judgment of tracks will lead to the inability of GM-PHD filter to track the targets that need attention. For PHD filter, accurate distinction of tracks is the key to ensure tracking performance [16–18]. In MTT, it is the premise of establishing the track on determining the identity of the target. The data association algorithm [19] proposed by Panta et al. provides a unique label for each target and obtains the track

of a single target through the state at each time and the association between the targets [20]. Vo et al. [21–23] also proposed label CBMeMBer filter and label multitarget Bayesian processing method, which effectively solved the track formation problem of RFS processing multitarget and belonged to the pioneering work of label RFS.

In many cases, combining the information collected by multiple sensors can improve the tracking performance. Distributed MTT algorithm has attracted a lot of attention recently because of its advantages of strong fault tolerance, high flexibility, and low computational burden compared with centralized fusion framework [24–28]. The latest method of distributed multisensor MTT is GCI [29, 30], also known as exponential mixed density (EMD) [31]. GCI fusion is equivalent to calculating and minimizing the density of Kullback-Leibler divergences [32, 33] (KLD) gains from local and avoids the problem of double calculation of common information [34]. In the past few years, many distributed RFS filters based on GCI fusion rules have been proposed [35–43], including PHD and CPHD filters [23], and the fusion density can be calculated in closed form. On the contrary, in the case of label-based RFS filter, the application of GCI fusion is not simple, because GCI fusion of label RFS density can only be calculated in a closed form under special circumstances [39]. Even if the fusion density can be calculated, its performance is very sensitive to the inevitable label inconsistency between different sensors [44].

Although GCI fusion rule has the advantage of avoiding double calculation, it has been observed that this fusion rule may be sensitive to high missed detection rate [45]. In fact, GCI fusion rules tend to keep only all tracks existing in local posterior. When the sensor has different FoV, this defect will be aggravated. Some new methods are proposed recently to deal with the target missing problem caused by different FoV in GCI fusion framework. For example, in [46], two possible solutions based on SMC-PHD filter were proposed to solve this problem. In the first method, particles from different sensors were combined only if they were considered to represent the same target. In the second method, particles corresponding to the same target were hierarchically clustered and used for state extraction. However, both methods were prone to estimation errors and underestimated the number of targets when adjacent targets appeared. In [47], a distributed fusion algorithm based on SMC-PHD filter was proposed, which abandoned the limitation of completely overlapping FoV and divided the received particles into ordinary particle set and external particle set. Based on GM-PHD filter, [48] proposed a solution to deal with different FoV under the background of simultaneous positioning and mapping. Specifically, the method of [49] was based on the idea of initializing all local PHD with uniform intensity in the whole area and modeled the uncertainty of target position in the unexplored area. A different solution was proposed in [49], which modified the traditional GCI fusion algorithm by considering the distance between Gaussian components. However, this method cannot solve the problem of false positives, and the cardinality is overestimated. Recently, some scholars have extended the labeled RFS filter to multisensors by using similar ideas [50–52], but it is more challenging to develop effective solutions under this filtering framework because possible label inconsistencies need to be considered.

In order to solve the target omission problem of distributed multisensor PHD filtering based on GCI fusion rules, a stable and effective fusion method is proposed in this paper, which makes the fusion results not affected by fusion mismatch in GCI-PHD fusion generated by multisensors with limited FoV. The method includes two parts: Firstly, by analyzing the GCI fusion mismatch caused by the limited field sensor, whether the Gaussian component falls into the field intersection area is divided and differentiated; secondly, the problem of label inconsistency in GCI fusion is analyzed. For the fusion of labels in the intersection area, the best match of labels is found by minimizing the label inconsistency index, and then GCI fusion is implemented. The targets not in the intersection area of FoV are directly added to the final multitarget state according to the state provided by each sensor and the labels.

The subsequent chapters are arranged as follows: the second section introduces the traditional PHD filtering and GCI fusion rules; the third section analyzes the problems in the GCI fusion process, including fusion mismatch analysis and label inconsistency analysis, and introduction, including the distinction of Gaussian components and the improvement of label fusion; Section 5 verifies the effectiveness of the algorithm through linear simulation experiments; Section 6 is the conclusion. Table 1 lists the acronyms in the text.

2. Background

For MTT, under the condition of missing detection and clutter, we focus on solving the problem of estimating the unknown number of target states through the measurement data provided by sensors. Assuming the location of the sensors is known, each sensor s has a finite FoV, defined as

$$FoV_s = \{x \in X:\ p_D^s(x) > 0\}. \tag{1}$$

Among them, p_D^s represents the detection probability of the sensor s in the limited field of view. And different sensors have different FoV (usually depending on sensor type, location, and orientation).

The detection range of the sensor s is denoted by FoV_s, and $R[\cdot]$ denotes the detection range that can be sensed by all sensors. Figure 1 below shows a sensing network consisting of two sensors; then the detection range of the first sensor is

$$FoV_1 = R[1] \cup R[3], \tag{2}$$

where $R[i]$ denotes the ith region, which satisfies $\forall i \neq j$, $R[i] \cap R[j] = \varnothing$. The whole detection region R can be expressed as

$$R = \bigcup_{i=1}^{3} R[i]. \tag{3}$$

2.1. PHD Filtering. Consider the following MTT scenario, where the target state set is $X_k = \{x_k^1, \cdots, x_k^{N_k}\}$ and the measurement set is $Z_k = \{z_k^1, \cdots, z_k^{M_k}\}$, where x_k^n and z_k^m

Table 1: List of notation.

MTT	Multitarget tracking
FoV	Field of view
GCI	Generalized covariance intersection
PHD	Probability hypothesis density
PDA	Probabilistic data association
MHT	Multiple hypothesis tracking
RFS	Random finite set
SMC	Sequential Monte Carlo
GM	Gaussian mixture
EMD	Exponential mixed density
KLD	Kullback-Leibler divergences

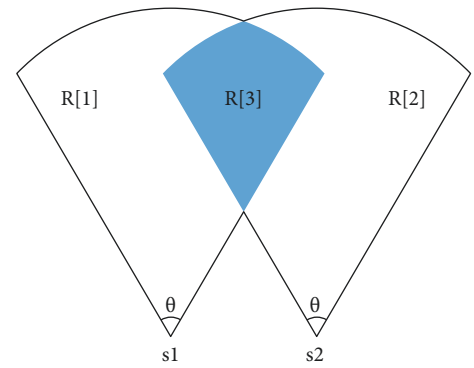

Figure 1: Distributed sensor network with limited field of view.

represent the nth target state and the mth measurement at time k, respectively. N_k and M_k are the number of targets and the number of measurements at time k, respectively. Assuming that the prior probability of multitarget approximately obeys Poisson distribution, with the help of random finite set statistics theory, the PHD recurrence equation [7] is

$$\begin{aligned} D_{k|k-1}(x) &= \int \left(p_{s,k|k-1} f_{k|k-1}(x|\zeta)\right) + \beta_{k|k-1}(x|\zeta) D_{k-1|k-1}(\zeta)\mathrm{d}\zeta + \gamma_k(x) \\ D_{k|k}(x) &= \left[1 - P_{D,k}\right] D_{k|k-1}(x) + \sum_{z_k \in Z_k} \frac{P_{D,k} g_k(z|x) D_{k|k-1}(x)}{\lambda c(z_k) + \int P_{D,k} g_k(z|\zeta) D_{k|k-1}(\zeta)\mathrm{d}\zeta}, \end{aligned} \tag{4}$$

$\gamma_k(x)$ and $\beta_{k|k-1}(x|\zeta)$ represent the target intensity of newborn and derived RFS, respectively [55], $p_{s,k|k-1}$ represent the survival probability of target at time $k-1$, and $p_{s,k|k-1} = p_{s,k-1}$, $P_{D,k}$ represent the detection probability of target at time k, $f_{k|k-1}(x|\zeta)$ represents the probability density function of state transition, $g_k(z|x)$ is the likelihood function of single target, λ is the average clutter number, and $c(z_k)$ obeys Poisson distribution. Poisson's RFS X multitarget density $\pi(X)$ takes the following form:

$$\pi(X) = \exp\left(-\int_X D(x)\mathrm{d}x\right) \prod_{x \in X} D(x). \tag{5}$$

Given a region $\chi \in X$, the number of prediction targets in the region can be calculated as $\int_{x \in \chi} D(x)\mathrm{d}x$, and the total number of prediction targets in the whole state space is $\int_X D(x)\mathrm{d}x$.

GM-PHD filter expresses the prior PHD and the posterior PHD of multiple targets as GM formation, and its iterative recursion can be expressed as a prediction update structure similar to Kalman filter (KF).

Assume that the multitarget posterior PHD at time $k-1$ can be expressed as GM, and the equation is as follows [53]:

$$D_{k-1}(x) = \sum_{i=1}^{J_{k-1}} w_{k-1}^i N\left(x; m_{k-1}^i, p_{k-1}^i\right), \tag{6}$$

where J_{k-1} is the number of Gaussian components at time $k-1$. w_{k-1}^i is the weight of the ith Gaussian component, and m_{k-1}^i and p_{k-1}^i present the mean and covariance of the ith Gaussian component.

The newborn and derived Gaussian components can be represented by a Gaussian mixture term [53]:

$$\begin{aligned} \gamma_k(x) &= \sum_{j=1}^{J_{\gamma,k}} w_{\gamma,k}^j N\left(x; m_{\gamma,k}^j, p_{\gamma,k}^j\right), \\ D_{\beta_{k|k-1}}(x) &= \sum_{j=1}^{J_{\beta,k}} w_{\beta,k}^j N\left(x; m_{\beta,k-1}^j, Q_{\beta,k-1}^j\right). \end{aligned} \tag{7}$$

Among them, $J_{\gamma,k}$ and $J_{\beta,k}$ represent the number of newborn and derived Gaussian components at time k, respectively. $w_{\gamma,k}^j$ and $w_{\beta,k}^j$ represent the weights of the newborn and derived j-th Gaussian components at time k, respectively. $m_{\gamma,k}^j$ and $p_{\gamma,k}^j$ are the mean and covariance of the j-th newborn Gaussian component, respectively. $m_{\beta,k-1}^j = F_{\beta,k-1}^j m_{k-1} + d_{\beta,k-1}^j$ and $Q_{\beta,k-1}^j$ are the mean and covariance of the j-th derived Gaussian component, respectively.

Then the multitarget prior PHD at time k can be expressed as [53]

$$D_{k|k-1}(x) = \gamma_k(x) + D_{\beta_{k|k-1}}(x) + D_{sv_{k|k-1}}(x), \tag{8}$$

where $D_{\beta_{k|k-1}}(x)$ and $D_{sv_{k|k-1}}(x)$ are the Gaussian mixture intensity functions of the derived and surviving targets, respectively, $J_{k|k-1}$ is the number of Gaussian components to predict PHD, w_{kk-1}^i, $m_{k|k-1}^i$, and $p_{k|k-1}^i$ are the weight, mean, and covariance of the ith Gaussian component in the predicted intensity function, respectively, w_k^j, m_k^j, and p_k^j are the update weights, mean, and covariance of the j-th component in the intensity function.

The derived Gaussian component intensity can be expressed as [53]

$$D_{\beta_{k|k-1}}(x) = \sum_{i=1}^{J_{k1|k-1}} \sum_{j=1}^{J_{\beta,k}} w_{k-1|k-1}^{i} w_{\beta,k}^{j} N\left(x; m_{\beta,k-1}^{i,j}, Q_{\beta,k-1}^{i,j}\right), \quad (9)$$

where

$$\begin{aligned} m_{\beta,k-1}^{i,j} &= F_{\beta,k-1}^{j} m_{k-1|k-1}^{i} + d_{\beta,k-1}^{j}, \\ Q_{\beta,k-1}^{i,j} &= F_{\beta,k-1}^{j} p_{k}^{i} \left(F_{\beta,k-1}^{j}\right)^{T} + Q_{\beta,k-1}^{j}. \end{aligned} \quad (10)$$

The surviving Gaussian component intensity can be expressed as [53]

$$D_{sv_{k|k-1}}(x) = p_{s,k|k-1} \sum_{i=1}^{J_{k-1|k-1}} w_{k-1|k-1}^{i} N\left(x; m_{sv,k|k-1}^{i}, p_{sv,k|k-1}^{i}\right), \quad (11)$$

where

$$\begin{aligned} m_{sv,k|k-1}^{i} &= F_{k-1} m_{k-1|k-1}^{i}, \\ p_{sv,k|k-1}^{i} &= F_{k-1} p_{k-1|k-1}^{i} F_{k-1}^{T} + Q_{k-1}, \end{aligned} \quad (12)$$

where F_{k-1} is the state transition matrix and Q_{k-1} is the process noise covariance. Then the k-time prior multitarget PHD can be expressed as a Gaussian mixture form [53].

$$D_{k|k-1}(x) = \sum_{i=1}^{J_{k|k-1}} w_{k|k-1}^{i} N\left(x; m_{k|k-1}^{i}, p_{k|k-1}^{i}\right). \quad (13)$$

Among them, $w_{k|k-1}^{i} = p_{s,k-1} w_{k-1|k-1}^{i}$ represents the prior weight from the posterior weight at time k-1. $J_{k|k-1} = J_{k-1|k-1}(1 + J_{\beta,k}) + J_{\gamma,k}$ represents the number of prior Gaussian components at time k.

Then, the posterior intensity at time k is as follows [53]:

$$\begin{aligned} D_{k}(x) &= \left[1 - P_{D,k}\right] D_{k|k-1}(x) \\ &\quad + \sum_{l=1}^{m_k} \sum_{i=1}^{J_{k|k-1}} w_{k|k}^{i}\left(z_{k}^{l}\right) N\left(x; m_{k|k}^{i,l}, p_{k|k}^{i,l}\right), \end{aligned} \quad (14)$$

where

$$w_{k|k}^{i}\left(z_{k}^{l}\right) = \frac{P_{D,k} w_{k|k-1}^{i} g_{k|k-1}\left(z|m_{k|k-1}^{i}, p_{k|k-1}^{i}\right)}{\lambda c\left(z_{k}^{l}\right) + P_{D,k} \sum_{j=1}^{J_{k|k-1}} w_{k|k-1}^{i} g_{k|k-1}\left(z|m_{k|k-1}^{j}, p_{k|k-1}^{i}\right)}, \quad (15)$$

$$K_{k}^{i} = \widehat{p}_{k|k-1}^{i} H_{k}^{T}\left[H_{k} \widehat{p}_{k|k-1}^{i} H_{k}^{T} + R_{k}\right]^{-1}, \quad (16)$$

$$\widehat{m}_{k}^{i} = \widehat{m}_{k|k-1}^{i} + K_{k}^{i}\left(z_{k}^{l} - H_{k} \widehat{m}_{k|k-1}^{i}\right), \quad (17)$$

$$\widehat{p}_{k|k}^{i} = \left[I - K_{k}^{i} H_{k}\right] \widehat{p}_{k|k-1}^{i}. \quad (18)$$

R_k is the measurement noise covariance matrix, and I is the identity matrix.

The number of predicted targets $\widehat{N}_{k|k-1}$ and $\widehat{N}_{k}$ associated with $D_{k|k-1}$ and D_k is obtained by the following equation [54]:

$$\begin{aligned} \widehat{N}_{k|k-1} &= \widehat{N}_{k-1}\left(p_{s,k} + \sum_{j=1}^{J_{\beta,k}} w_{\beta,k}^{j}\right) + \sum_{j=1}^{J_{\gamma,k}} w_{\gamma,k}^{j}, \\ \widehat{N}_{k} &= \widehat{N}_{k|k-1}\left(1 - p_{D,k}\right) + \sum_{z \in Z_k} \sum_{j=1}^{J_{k|k-1}} w_{k}^{j}(z), \end{aligned} \quad (19)$$

where $J_{\beta,k}$ and $J_{\gamma,k}$ represent the number of derived Gaussian components and newborn Gaussian components at time k, respectively. Therefore, at time k, the number of Gaussian components of D_k is $J_k = (J_{k-1}(1 + J_{\beta,k}) + J_{\gamma,k})(1 + |Z_k|)$.

2.2. GCI Fusion Rules. $\pi_k^1(X)$ and $\pi_k^2(X)$ of two multitarget posterior probability density functions are considered based on the measurement sets from two different sensors. When the correlation between two measurement sets is unknown, two multitarget posteriori can be fused by GCI fusion rule [29]. Under GCI fusion rule, two multitarget posterior probability density functions are fused to obtain

$$\pi_k^{1,2}(X) = \frac{\pi_k^1(X)^{\omega_1} \pi_k^2(X)^{\omega_2}}{\int \pi_k^1(X)^{\omega_1} \pi_k^2(X)^{\omega_2} \delta X}, \quad (20)$$

where ω_1 and ω_2 are the weights that determine the relative importance of each multitarget posteriori, satisfying $\omega_1 + \omega_2 = 1$. One method of weight selection is the Metropolis weight selection method [55]. It can guarantee fusion convergence. Another method is to select the cost function that minimizes the target weights according to the optimization process [56]. The fusion density provided by the fusion rule (20) is a minimization of the weighted sum of the KLD with respect to the density to be fused.

$$\pi_k^{1,2} = \arg\inf_{\pi}\left(\omega_1 D_{KL}\left(\pi \| \pi_k^1\right) + \omega_2 D_{KL}\left(\pi \| \pi_k^2\right)\right). \quad (21)$$

Among them

$$D_{KL}\left(\pi \| \pi_k^i\right) \triangleq \int \pi(X) \log \frac{\pi(X)}{\pi^i(X)} \delta X. \quad (22)$$

The density of N_s multitargets and their corresponding fusion weights are paired into a set; that is, $\prod = (\pi_s, \omega_s)_{s \in N_s}$; GCI divergence $G(\prod)$ is defined as [57]

$$G\left(\prod\right) = \min_{\pi} \sum_{s \in N} \omega_s D_{KL}(\pi \| \pi_s) = -\log c\left(\prod\right). \quad (23)$$

Among them

$$c\left(\prod\right) = \int \prod_{s \in N} \left[\pi_s(X)\right]^{\omega_s} \delta X, \quad (24)$$

where the GCI coefficient $c(\prod)$ satisfies $0 < c(\prod) < 1$.

For simplicity, only two sensors are considered.

According to GCI fusion rules, Poisson RFS with PHDs $D_k^1(x)$ and $D_k^2(x)$ are fused to produce a Poisson RFS fused with PHD

$$D_k^{1,2}(x) = \left[D_k^1(x)\right]^{\omega_1} \left[D_k^2(x)\right]^{\omega_2}. \quad (25)$$

When PHD is represented by GM, the above results cannot be calculated in closed form because the exponent of GM cannot be GM, so there is an approximation strategy to approximate each power $[D_k^l(x)]^{\omega_l}$ to a GM. For example,

$$\left[D_k^l(x)\right]^{\omega_l} = \sum_{i=1}^{N^l} \widetilde{\alpha}_{k,i}^l N\left(x; \widetilde{m}_{k,i}^l, \widetilde{p}_{k,i}^l\right), \tag{26}$$

where $\widetilde{m}_{k,i}^l$ is the mean of the ith Gaussian component of sensor l at time k, $\widetilde{p}_{k,i}^l$ is the covariance of the ith Gaussian component of sensor l at time k, and $\widetilde{\alpha}_{k,i}^l$ is the weight of the ith Gaussian component of sensor l at time k. Then, compute the fusion PHD

$$D_k^{1,2}(x) = \sum_{i=1}^{N^1} \sum_{j=1}^{N^2} \alpha_{k,i,j}^{1,2} N\left(x; m_{k,i,j}^{1,2}, p_{k,i,j}^{1,2}\right). \tag{27}$$

Among them

$$p_{k,i,j}^{1,2} = \left[\left(\widetilde{p}_{k,i}^1\right)^{-1} + \left(\widetilde{p}_{k,j}^2\right)^{-1}\right]^{-1}, \tag{28}$$

$$m_{k,i,j}^{1,2} = p_{k,i,j}^{1,2}\left[\left(\widetilde{p}_{k,i}^1\right)^{-1} \widetilde{m}_{k,i}^1 + \left(\widetilde{p}_{k,j}^2\right)^{-1} \widetilde{m}_{k,j}^2\right], \tag{29}$$

$$\alpha_{k,i,j}^{1,2} = \widetilde{\alpha}_{k,i}^1 \widetilde{\alpha}_{k,j}^2 N\left(\widetilde{m}_{k,i}^1 - \widetilde{m}_{k,j}^2; 0, \widetilde{p}_{k,i}^1 + \widetilde{p}_{k,j}^2\right). \tag{30}$$

$m_{k,i,j}^{1,2}$, $p_{k,i,j}^{1,2}$, and $\alpha_{k,i,j}^{1,2}$ are the mean, covariance, and weight of the fused Gaussian components, respectively.

3. Problem Analysis

3.1. GCI Fusion Mismatch Analysis. This paper analyzes the situation of GCI fusion when it is applied to different *FoV* sensors by actual scene and discusses the reasons why GCI fusion may fail in this case.

Considering a distributed sensor network with two sensors, GM-PHD filtering is used for tracking. The observation area is $[-2000, 2000] \times [0, 2000]\,(\mathrm{m}^2)$. For simplicity, the two targets move in a circle. The survival probability is $p_{s,k} = 0.99$, and the positions of the two sensors are $p_1 = [-1000, 0]^T$, $p_2 = [500, 0]^T$.

Each sensor has a limited *FoV*, which can only detect targets with relative angles in the interval $[-60^\circ, 60^\circ]$. Detect probability $p_{D,k} = 0.98$ in *FoV*; otherwise it is 0. The true trajectory is shown in Figure 2, and the cardinality estimation is shown in Figure 3.

As can be seen from Figure 2, Target 1 can only be detected by Sensor 1, and Target 2 can only be detected by Sensor 2. Therefore, the PHD of Sensor 1 does not contain a Gaussian component representing Target 2, whereas the PHD of Sensor 2 does not contain a Gaussian component representing Target 1, and the Gaussian component of Sensor 1 and the Gaussian component of the Sensor 2 are far apart. The result is that the tracking performance after fusion is obviously worse than that of a single sensor, and the number of targets after fusion is 0.

The essence of GCI fusion rule is the weighted multiplication between target densities. Only when both sensors detect the same target can the fusion process proceed normally. When a sensor does not detect a target, its PHD would approach zero in the corresponding region of the state space. Even if another sensor can detect the target and there are Gaussian components with nonnegligible weights in this region, the application of GCI fusion rules would significantly reduce such weights. Targets may be lost in the fused multitarget distribution, as happens in simulation. It can also be seen from GCI fusion, implemented based on the GM method (18), that large distances between Gaussian components result in small fusion weights because $N(\widetilde{m}_{k,i}^1 - \widetilde{m}_{k,j}^2; 0, \widetilde{p}_{k,i}^1 + \widetilde{p}_{k,j}^2)$ tends to zero as $\widetilde{m}_{k,i}^1 - \widetilde{m}_{k,j}^2$ increases.

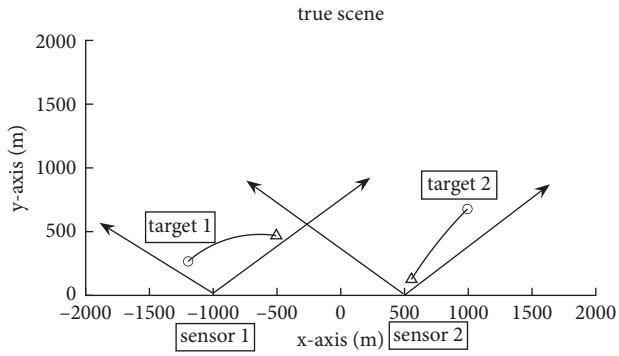

Figure 2: Real track.

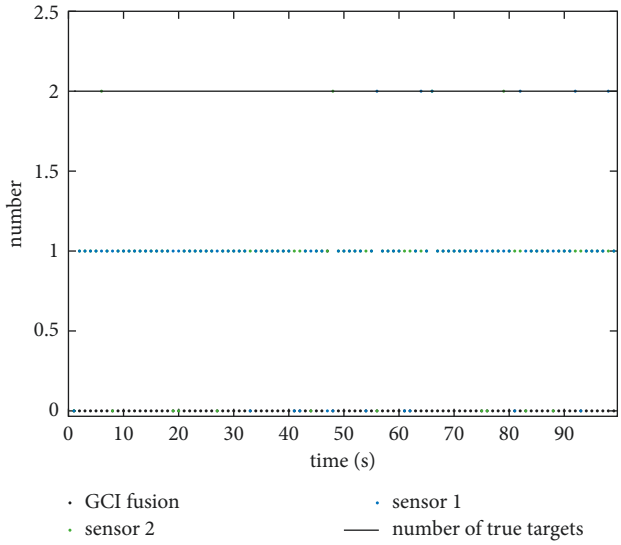

Figure 3: Estimated number of targets.

3.2. Label Inconsistency Analysis. In addition to PHD fusion, in order to form continuous tracks, Gaussian components also carry corresponding label information [57], so it is also necessary to fuse corresponding labels, and each Gaussian component is assigned a unique label

$$\Gamma_0 = \left\{\tau_0^1, \ldots, \tau_0^{J_k}\right\}, \tag{31}$$

τ_0^i represents the label of the ith Gaussian component.

Due to the inherent hypothesis of complete consistency between labels of different sensors, the parallelization of GCI

is actually realized. However, as pointed out in [57], it is precisely because of this inherent hypothesis that when labels are inconsistent, the performance of GCI fusion would drop sharply, which is called label inconsistency. Label inconsistency means that the same target is assigned different labels in different sensors.

In practice, even if the local filter works well, GCI fusion may not produce accurate results because the hypothesis of label consistency is difficult to guarantee. There are many reasons for label inconsistency, such as uncertainty in measurement, that is, noise, clutter, and low detection probability; take local pruning operation, etc.

Consider a set of multitarget densities and corresponding weights $\prod = \{(\pi_s, \omega_s)\}_{s\in N}$, where each π_s is defined in $F(X \times \tau_s)$ and supports $F(X \times \Gamma_s)$. Each π_s is an unlabeled version of π_s; given a set of unlabeled target states, and $x_1, \cdots, x_n$, the label information is described by the conditional joint probability distribution of its corresponding label $\tau_1, \cdots, \tau_n$.

$$\varpi(\{(\tau_1|x_1), \ldots, (\tau_n|x_n)\}) = \frac{\boldsymbol{\pi}(\{(\tau_1|x_1), \ldots, (\tau_n|x_n)\})}{\pi(\{x_1, \ldots, x_n\})}. \tag{32}$$

Among them, $\pi(\{x_1, \ldots, x_n\})$ accords the following marginal distribution [58].

$$\pi(\{x_1, \ldots, x_n\}) = \sum_{(\alpha_1,\ldots,\alpha_n)\in\Gamma^n} \boldsymbol{\pi}(\{(x_1|\alpha_1), \ldots, (x_n|\alpha_n)\}). \tag{33}$$

For n object states $x_1, \ldots, x_n$, they are labeled as Γ^n, and each marked mode can be expressed as a vector $(\alpha_1, \ldots, \alpha_n) \in \Gamma^n$; that is, x_i is represented as α_i, and $\varpi(\{(\tau_1|x_1), \ldots, (\tau_n|x_n)\})$ denotes the probability of the possible hypothesis label $(\tau_1, \cdots, \tau_n)$ for state $x_1, \cdots, x_n$

Using the GCI coefficient $\varpi_s(\{(\tau_1|x_1), \cdots, (\tau_n|x_n)\}), s \in N$ between multiple conditional multilabel distributions, for a given set of unlabeled state $x_1, \cdots, x_n$, the label inconsistency can be described as

$$\begin{aligned}\mu_\Pi &= (\{x_1, \ldots, x_n\}) \\ &= \sum_{(\tau_1,\ldots,\tau_n)\in\Gamma^n} \prod_{s\in N} [\varpi_s(\{(\tau_1|x_1), \ldots, (\tau_n|x_n)\})]^{\omega_s}.\end{aligned} \tag{34}$$

According to the distribution of X represented by the fusion density $\pi_w(\cdot)$ returned by the GCI fusion of $\prod = \{(\pi_s, \omega_s)\}_{s\in N}$, the statistical average of GCI coefficient $\mu_\Pi(X)$ in the state space is taken, where each π_s is unlabeled. The following label inconsistencies are defined according to [57].

Definition 1. The label inconsistency index between the multitarget densities of labels in Π is defined as

$$d_G(\boldsymbol{\Pi}) \triangleq G(\boldsymbol{\Pi}) - G(\Pi) = -\log E_{\pi_\omega}[\mu_\Pi(X)], \tag{35}$$

wherein $E_{\pi_\omega}(\cdot)$ is an expectation with respect to the probability density π_ω, i.e., the fusion density returned from the density in GCI fusion.

Introducing target probability and nontarget probability into [23]

$$\begin{aligned}P_y(\pi) &= 1 - \pi(\varnothing), \\ P_n(\pi) &= \pi(\varnothing),\end{aligned} \tag{36}$$

where π denotes a posterior density. Only when the probability of the target is greater than the given threshold can the target be recognized as existing. GCI fusion π_ω of matched labels can be written as the target probability of GCI fusion π_ω of corresponding unmatched labels [57]:

$$P_y(\pi_\omega) = 1 - e^{d_G(\boldsymbol{\Pi})}\left[1 - P_y(\pi_\omega)\right]. \tag{37}$$

The following inequality holds [57].

$$0 \le P_y(\boldsymbol{\pi}_\omega) \le P_y(\pi_\omega). \tag{38}$$

These results show that given that $P_y(\pi_\omega)$ and $P_y(\pi_\omega)$ decrease exponentially with the increase of label inconsistency index $d_G(\Pi)$, when the target probability $P_y(\pi)$ is lower than a given threshold [59], the GCI fusion of Π cannot judge the existence of the target, so the GCI fusion performance of label multitarget density is very sensitive on $d_G(\Pi)$.

4. Solutions

4.1. Distinguish Gaussian Components. Based on the analysis in Section 3.1, Gaussian components need to be treated differently. The specific measure is to divide Gaussian components according to whether they only enter the FoV of one sensor but not the intersection of the FoV of the sensor.

Suppose $g_s^m = \{w_s^m, m_s^m, p_s^m\}, s = i, j$, so $G_i = \{g_i^m\}_{m=1,\cdots,J_i}$ and $G_j = \{g_j^n\}_{n=1,\cdots,J_j}$ represent the Gaussian components obtained by sensors i and j, respectively. The Gaussian component from the sensor i but not in the FoV intersection range is obtained by the following equation:

$$G_i^D = \left\{g_i^m \in G_i | m_i^m \notin FoV_j\right\}. \tag{39}$$

The remaining components are given by the following equation:

$$G_i^C = G_i - G_i^D. \tag{40}$$

Similarly, the Gaussian component from the sensor j but not in the FoV intersection range is obtained by the following equation:

$$G_j^D = \left\{g_j^m \in G_j | m_j^m \notin FoV_i\right\}. \tag{41}$$

The remaining components are given by the following equation:

$$G_j^C = G_j - G_j^D. \tag{42}$$

After obtaining the segmented Gaussian component, G_i^C and G_j^C are fused according to equation (17), and the resulting fused PHD is expressed as $\overline{D}_*^C$. In addition, the remaining G_i^D and G_j^D corresponding PHD are represented D_j^D by D_i^D and D_j^D, and the final PHD fusion can be expressed as

$$\overline{D}_0 = \overline{D}_*^C + D_i^D + D_j^D. \tag{43}$$

This means that the PHD fuses only for the Gaussian components from G_i^C and G_j^C, while the Gaussian components corresponding to the G_i^C and G_j^C are added directly to the fused PHD.

4.2. Improved Label Fusion. In the range of multisensor FoV intersection, besides PHD fusion, label inconsistency in the fusion process should also be considered. As mentioned earlier, when labels are inconsistent between different sensors, the traditional GCI fusion performance of label multitarget density would deteriorate. An effective solution to solve label inconsistency is to match labels with different posterior PHD when fusing posterior PHD from different sensors at every moment, so that the same label corresponds to the same target when fusing labels.

Fusion of two label multitarget posterior PHD from sensor a and sensor b is considered, respectively. Two PHD posteriors are paired with their corresponding fusion weights and are collected into a set, which is represented by $\{(\omega_a, \pi_a), (\omega_b, \pi_b)\}$. The definition of label matching describing the corresponding hypothesis between two node labels is given below.

A label matched from a label in L_a to a label in L_b is defined as bijective ς: $L_a \longrightarrow L_b$, where L_a and L_b represent the label space of sensor a and sensor b, respectively. The set of all these label matches, denoted as $\Gamma(L_a, L_b)$, is called the label match space for L_a and L_b. For any subset $I \subseteq L_a$, define $\varsigma(I) \triangleq \cup_{l \in I} \varsigma(l)$ and $\varsigma(l)$ as images of l.

Label matching should be defined over the entire label space because a nonzero probability label of one sensor may correspond to a zero probability label of another sensor. For example, due to random error detection by one sensor, a label with a probability less than the threshold can be trimmed or truncated, while it may have a high probability in the corresponding label of another sensor because the other sensor can detect it well.

Each label matching hypothesis is the hypothesis that ς represents each label l of sensor a corresponding to a label $\varsigma(l)$ of sensor b, which represent the same target. In order to ensure the consistency of labels between sensor a and sensor b, a feasible method is to relabel the label multitarget state X of one sensor by using the labeling method of another sensor.

Sensor a is used as a reference point and sensor b is used as a relabeled sensor. Under the hypothesis ς of label matching, the label multitarget state $\{(x_1, l_1), \ldots, (x_n, l_n)\}$ of sensor b is relabeled by the labeling mode of sensor a, and the labeled multitarget state can be expressed as $\{(x_1, l_1), \ldots, (x_n, l_n)\}$. Therefore, the label multitarget posterior representation of the relabeled sensor b is expressed as $\pi_b^{(\varsigma)}(X)$, and the function is

$$\begin{aligned} &\boldsymbol{\pi}_b^{(\varsigma)}(\{(x_1, l_1), \ldots, (x_n, l_n)\}) \\ &\quad = \boldsymbol{\pi}_b(\{(x_1, \varsigma(l_1)), \ldots, (x_n, \varsigma(l_n))\}). \end{aligned} \tag{44}$$

The statistical data of the state of the unlabeled object before and after the relabeling remains unchanged because the unlabeled data of $\pi_b(X)$ and $\pi_b^{(\varsigma)}(X)$ are identical according to equation (33); i.e., the relabeling process changes only the label information described by the conditional multilabel distribution.

In order to evaluate the quality of label matching, the label inconsistency index in equation (29) is used to measure the difference of label information in $\pi_a(X)$ and $\pi_b^{(\varsigma)}(X)$. Then, the best label matching with ς is selected as the index of minimizing label inconsistency $d_G(\{\pi_a, \omega_a\}, \{\pi_b^{(\varsigma)}, \omega_b\})$, that is,

$$\varsigma^* = \arg \min_{\varsigma \in \Gamma(L_a, L_b)} d_G\left(\{\boldsymbol{\pi}_a, \omega_a\}, \left\{\boldsymbol{\pi}_b^{(\varsigma)}, \omega_b\right\}\right). \tag{45}$$

Minimization (35) is equivalent to reducing the adverse effects of label inconsistencies on GCI fusion. Once an optimal match ς^* is obtained, GCI fusion of $\pi_a(X)$ and $\pi_b^{(\varsigma^*)}(X)$ is performed on the label state space, thereby returning the fusion density $\pi_\omega(X)$.

This means that the target labels and states are fused by GCI in the intersection range of sensors' FoV, while the targets outside the intersection range are directly added to the final fused multitarget states according to the states and labels provided by each sensor.

5. Simulation Verification

5.1. Experimental Parameter Setting. In the simulation, GM-PHD filter is used to verify the tracking performance of the proposed fusion algorithm, and the proposed fusion algorithm *FoV* is carried out in a finite linear sensor. In order to verify the effectiveness of the proposed algorithm in MTT scene, the improved GCI-GM-PHD algorithm is compared with the traditional GCI-GM-PHD algorithm, and the finite FoV Sensor 1 using GM-PHD filter and the finite FoV Sensor 2 by GM-PHD filter are compared. The experimental parameters are set as follows.

The tracking scene is set to multiple targets in four possible locations or derived from other targets, and the observation area is $[-1000, 1000] \times [-1000, 1000]\,(\mathrm{m}^2)$. There are six targets in the scene. For simplicity, it is assumed that each target moves in a straight line at a uniform speed.

The state vector of the target consists of position and velocity components: $x_k = [p_{x,k} p_{y,k} v_{x,k} v_{y,k}]$, and its state equation is

$$x_k = \begin{bmatrix} 1 & 0 & T & 0 \\ 0 & 1 & 0 & T \\ 0 & 0 & 1 & 0 \\ 0 & 0 & 0 & 1 \end{bmatrix} x_{k-1} + \begin{bmatrix} \frac{T^2}{2} & 0 \\ 0 & \frac{T^2}{2} \\ T & 0 \\ 0 & T \end{bmatrix} w_{k-1}. \tag{46}$$

The sampling interval T is 1 s, the total tracking time is 100 s, and the process noise is $w_k \sim N(0,5)$. The intensity of new target is as follows:

$$\gamma_k(x) = \sum_{i=1}^{4} \omega_{\gamma,k}^{i} N\left(x; m_{\gamma,k}^{i}, p_{\gamma,k}^{i}\right). \tag{47}$$

Among them, $m_{\gamma,k}^{1} = [0;0;0;-10]^T$, $m_{\gamma,k}^{2} = [0;400;3;-7]^T$, $m_{\gamma,k}^{3} = [-800;-800;3;15]^T$, and $m_{\gamma,k}^{4} = [600;100;15;-5]^T$. The weights of new target $\omega_{\gamma,k}^{i} = 0.03$, the process noise of new targets obeys Gaussian distribution, and the mean value is zero. The covariance is $Q_{sp,k}^{i} = \mathrm{diag}([100,100,100,100])$.

In the Gaussian component pruning and merging section, the truncation threshold of the Gaussian component is set to 10^{-5}. The state extraction threshold is set to 0.5, the merging threshold is set to 10, and the maximum number of Gaussian components is 100. The number of Monte Carlo simulations is 100. Evaluating tracking quality by OSPA distance:

$$\mathrm{OSPA}_{p,c}(x_k, \hat{x}_k) = \sqrt[p]{\frac{\min \sum_{i=1}^{|x_k|} \left(d_c\left(x_k^i, \hat{x}_k^{\pi(i)}\right)\right)^p + c^p\left(|\hat{x}_k| - |x_k|\right)}{|\hat{x}_k|}}. \tag{48}$$

x_k is the target state vector; the two parameters of OSPA distance are set to $p = 1$ and $c = 200$, respectively. The smaller the OSPA distance, the higher the accuracy of target state estimation.

Two sensors are located at $(-500\,\mathrm{m}, -1000\,\mathrm{m})$ and $(500\,\mathrm{m}, -1000\,\mathrm{m})$, respectively, which provide measurements of unknown targets. Each sensor has a limited FoV with a detection radius of 2000 m, which can only detect targets with relative angles in the interval $[-60^\circ, 60^\circ]$. In FoV, the detection probability is constant; that is,

$$p_D^s = \begin{cases} 0.95, & x \in FoV_s, \\ 0, & x \notin FoV_s. \end{cases} \tag{49}$$

For $s = 1, 2$, the measurement vector is position information: $z_k = [p_{z_x,k}\, p_{z_y,k}]$; the measurement equation is given by the following equation:

$$z_k = \begin{bmatrix} 1 & 0 & 0 & 0 \\ 0 & 1 & 0 & 0 \end{bmatrix} x_k + v_k, \tag{50}$$

where noise is measured as $v_k \sim N(0,5)$. Clutter follows uniform Poisson RFS, with an average of 60 clutter points per scan ($\lambda = 60$).

5.2. Simulation Results. Figure 4 shows a simulated multi-target motion scene in which the target has cross motion, Target 1 is in the detection field of Sensor 1 but not in the detection field of Sensor 2, and Target 2 is in the detection field of Sensor 2 but not in the detection field of Sensor 1.

Figure 5 shows the tracking results of Sensor 1 in a limited FoV. The black solid line in the figure is the real trajectory of the target, the colored points are the estimation of the target trajectory by the sensor, and the dense gray points are the measurements. It can be clearly seen that

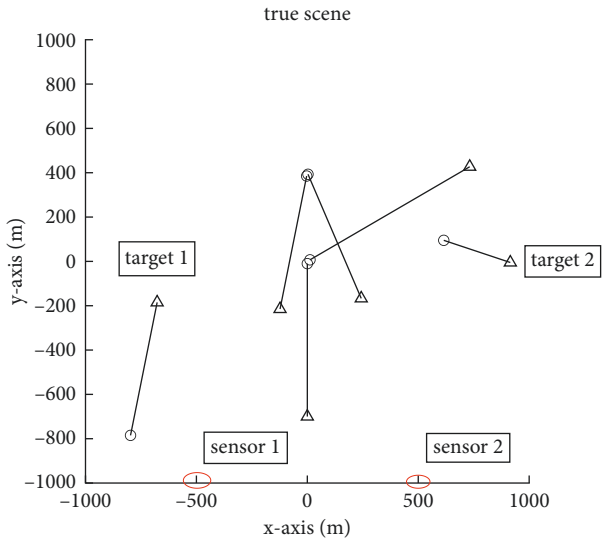

Figure 4: Real target trajectory.

Target 2 is completely lost by Sensor 1, because the estimation of the sensor does not appear on its true trajectory. Sensor 1 and Sensor 2 use traditional GM-PHD filters. Due to the influence of clutter, clutter points will be regarded as real targets, and label allocation will become blurred and unclear when targets move across. Figure 6 shows the tracking result of Sensor 2 under limited FoV. Its tracking result is similar to that of Sensor 1, and the tracking of Target 1 is lost. When the target moves across, the estimated value will become uncertain, and the trajectory of the target will be temporarily lost.

Figure 7 shows the tracking results of two sensors fused by traditional GCI algorithm. It can be seen that the target tracking performance in the intersection of two sensors' FoV will be improved by using traditional GCI algorithm, but there will be a phenomenon of wrong label allocation. Traditional GCI fusion algorithm will directly lose Target 1 and Target 2 outside the intersection of two sensors' FoV. The reason is that Sensor 1 loses tracking Target 2 and Sensor 2 loses tracking Target 1, which directly leads to the loss of Target 1 and Target 2 in the fusion process.

Figure 8 shows the tracking result of fusing two sensors with the improved GCI algorithm. It can be seen that not only is the tracking effect of the target in the intersection range of the two sensors' FoV better, but also the phenomenon of inconsistent labels does not appear when the target crosses, and the tracking effect of the improved GCI fusion algorithm for Target 1 and Target 2 is still preserved outside the intersection range of the two sensors' FoV.

Figures 9 and 10 show OSPA distance comparisons and position comparisons for Sensor 1, Sensor 2, the traditional GCI-GM-PHD algorithm, and the improved GCI-GM-PHD algorithm, respectively. Target 1 starts to move from 60 seconds, and Target 2 starts to move from 80 seconds. From the OSPA distance comparison in Figure 8, it can be seen that the error of Sensor 1 increases sharply at 80 seconds, Sensor 2 increases sharply at 60 seconds, and GCI fusion algorithm also increases sharply at 60 seconds, because the

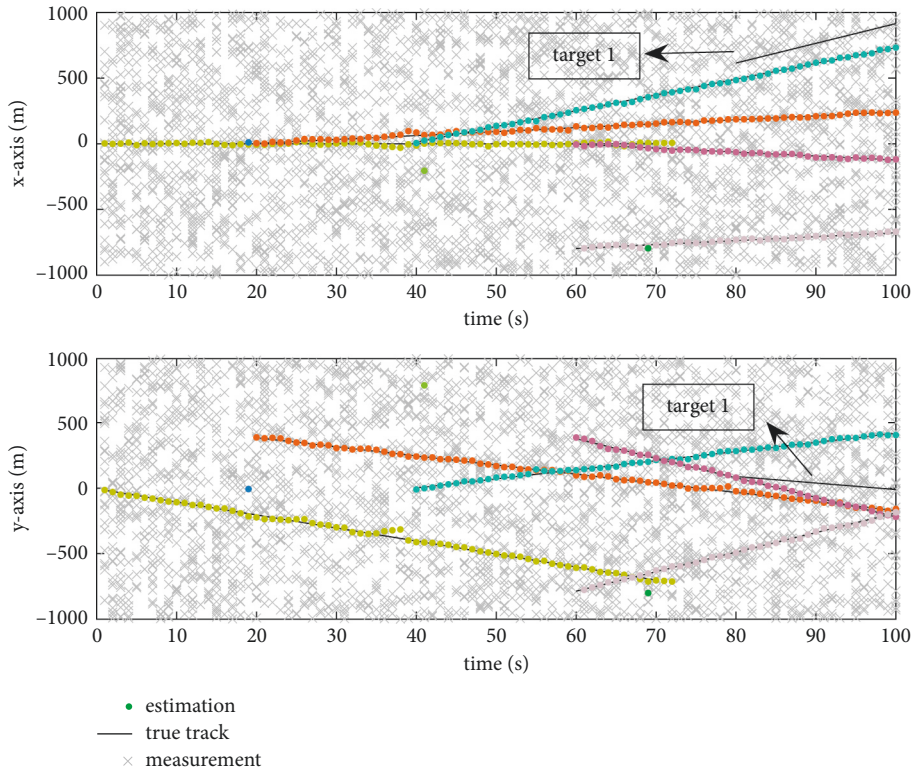

Figure 5: Tracking result of Sensor 1.

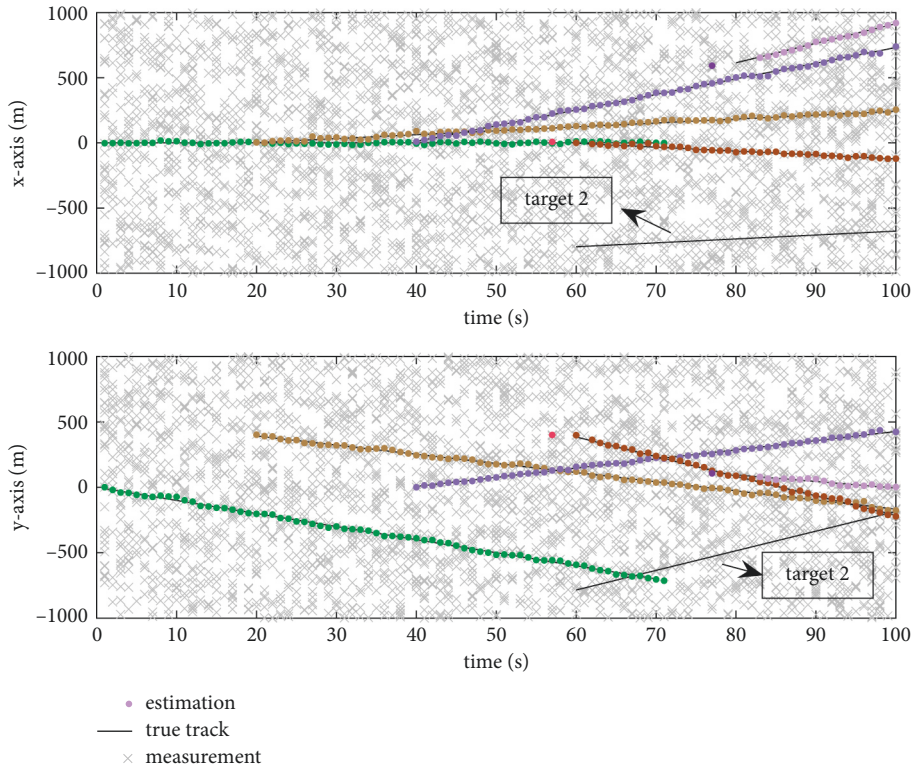

Figure 6: Sensor 2 tracking results.

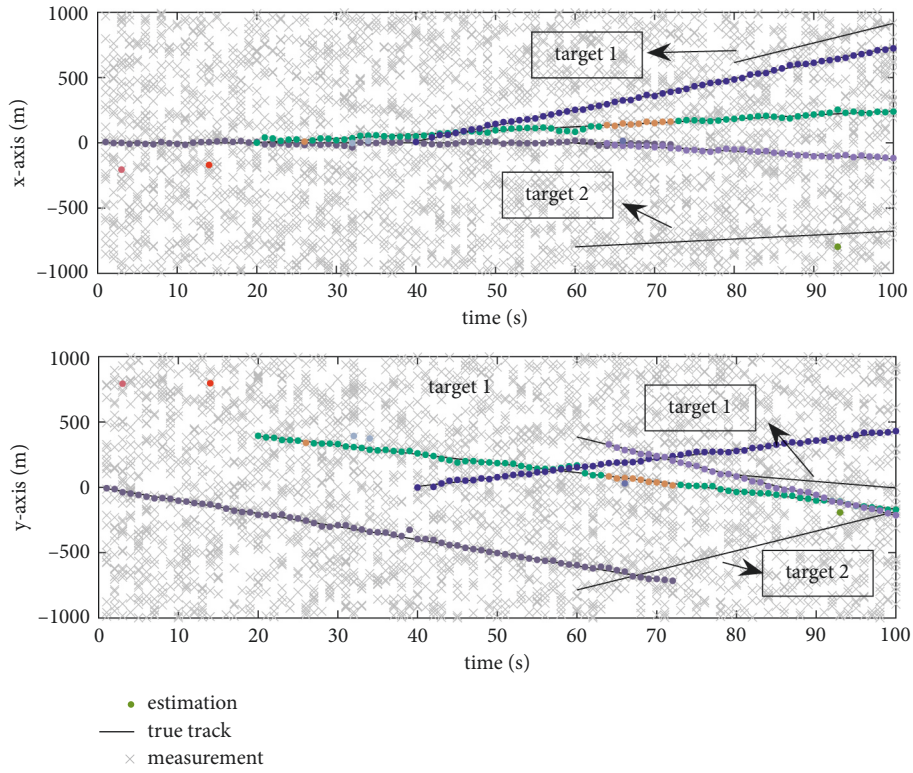

Figure 7: GCI-GM-PHD tracking results.

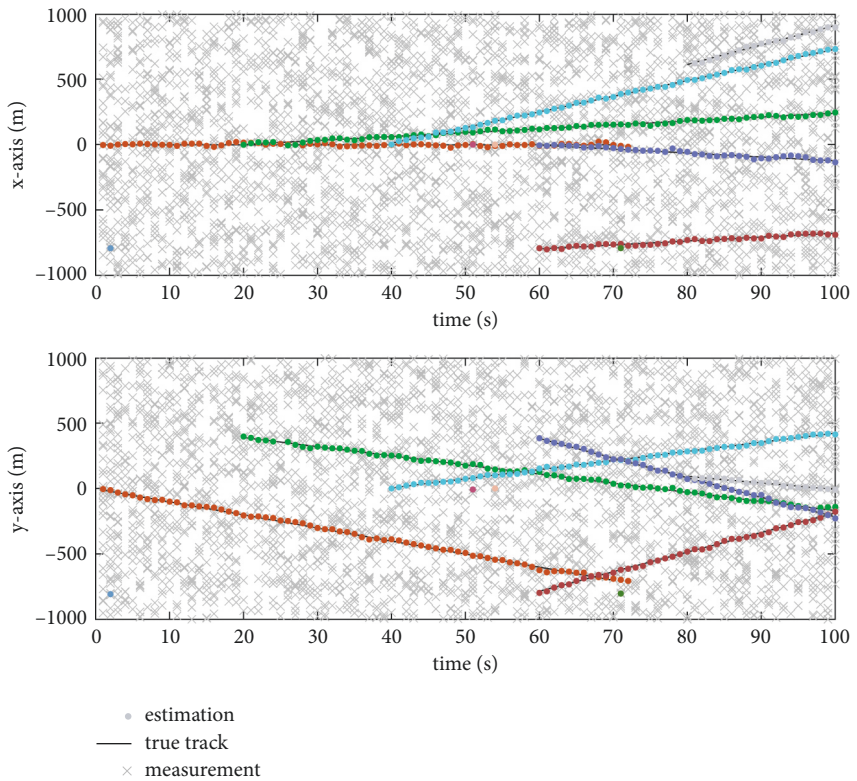

Figure 8: Improved GCI-GM-PHD tracking results.

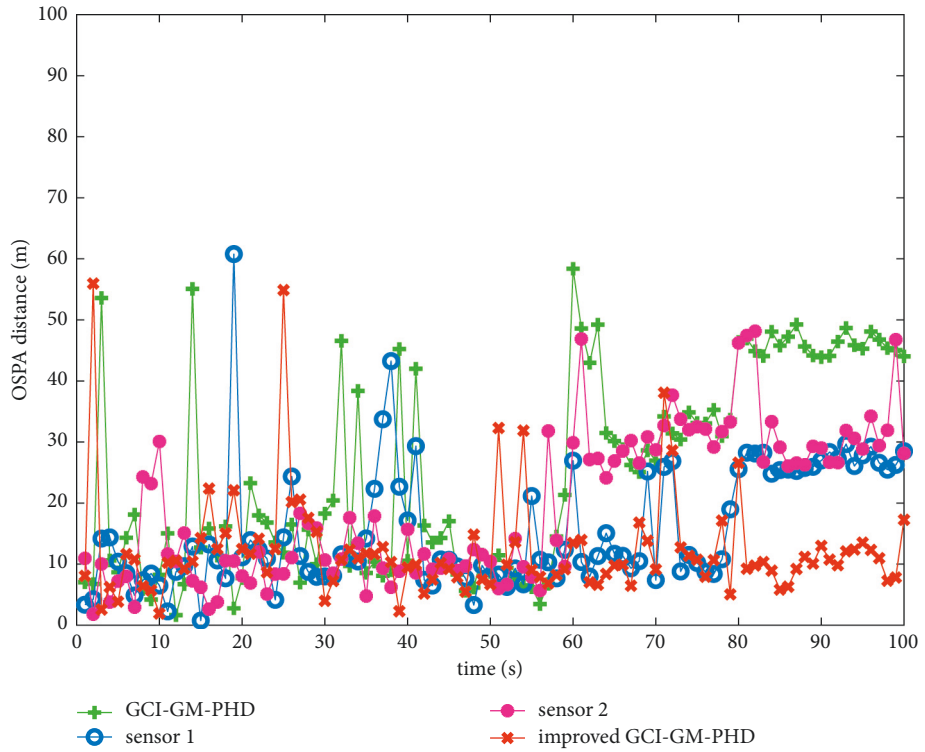

Figure 9: OSPA distance comparison chart.

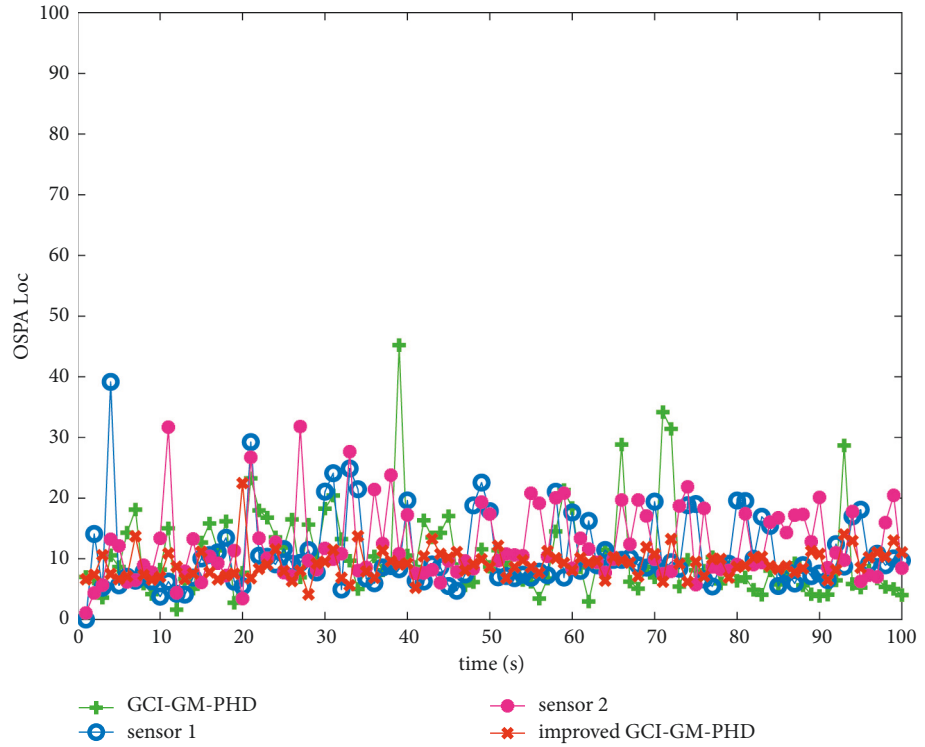

Figure 10: OSPA location comparison chart.

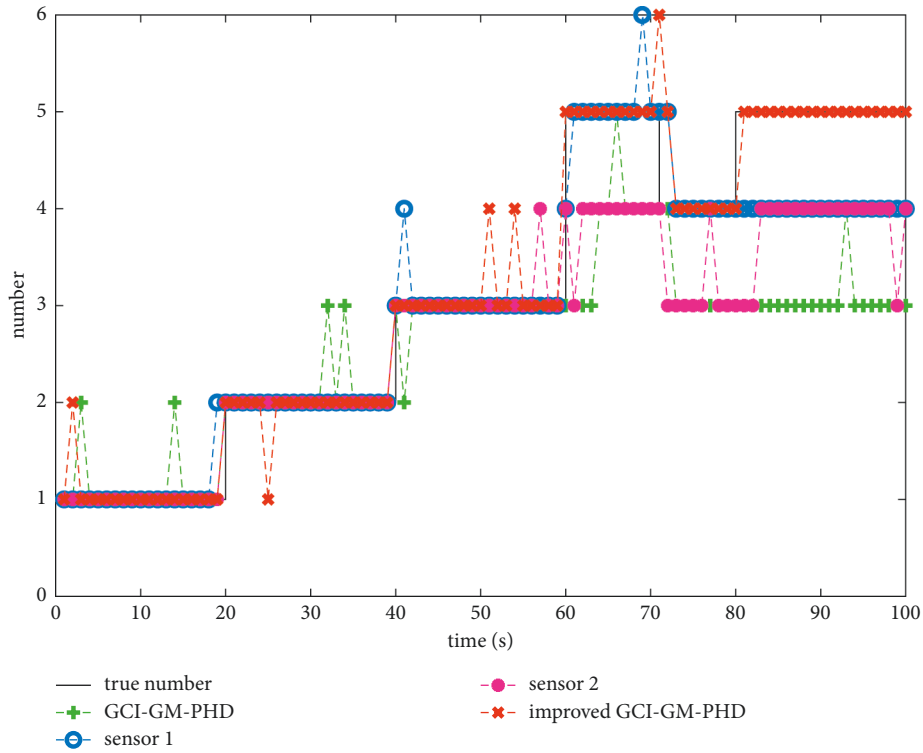

Figure 11: Comparison of target number estimation.

target information of the two sensors is inconsistent. The improved GCI fusion algorithm avoids this problem and still keeps a low error after 60 seconds. Due to the clutter, the error of the traditional GM-PHD filter will still increase sharply. In the follow-up research, we can consider improving the filter used in the sensor. It can be seen from Figure 10 that the position error of the improved GCI fusion algorithm is the lowest, which also directly proves the improvement of tracking performance of the improved fusion algorithm.

Figure 11 shows a comparison of target number estimates for Sensor 1, Sensor 2, the traditional GCI-GM-PHD algorithm, and the improved GCI-GM-PHD algorithm. It can be seen from the results in Figure 10 that the target number estimation results are consistent with the OSPA distance comparison results. Sensor 1 has a decrease in the target number estimation at 80 seconds, Sensor 2 has a decrease in the estimated number at 60 seconds, and traditional GCI fusion algorithm has a decrease in the number estimation at 60 seconds, while two targets are missed at 80 seconds. However, the improved GCI fusion algorithm performs well in target estimation, and there is no target loss. Figure 12 shows the potential estimation error comparison diagram of Sensor 1, Sensor 2, traditional GCI-GM-PHD algorithm, and improved GCI-GM-PHD algorithm, which also reflects the error of target number estimation result from another angle and verifies the improvement of tracking performance of improved GCI fusion algorithm.

5.3. Algorithm Performance Comparison Simulation after the Number of Targets Increases. In order to verify whether the proposed algorithm in this paper can be adapted to the case of more targets, 12 targets are added in scenario three, and the maximum number of targets surviving at the same time is 10. The clutter rate $\lambda = 30$, a set of single-sensor experiments are added to the simulation, assuming that it has an infinite field of view, and GM-PHD filtering is used to compare the performance of different algorithms, and other parameters settings are the same as 5.1. The simulation results are shown in Figures 13 and 14.

As shown in Figure 13(b), in the case of the increasing number of targets, the algorithm in this paper as a whole achieves well the target tracking effect after increasing the number of targets, despite the occurrence of mistakenly treating the clutter points as targets.

From Figures 14(a) and 14(b), it can be seen that the algorithm proposed in this paper can be well adapted to the situation where the number of targets increases. In terms of OSPA error, the algorithm in this paper shows the best performance. From Figures 14(c) and 14(d), it can be seen that the algorithm in this paper is significantly better than the remaining two algorithms in terms of target number estimation, which indirectly proves the stability of the algorithm in this paper in the case of the increasing number of targets.

The stability of each algorithm is added in this scenario for different clutter rates and different detection probabilities. From Figures 15(a) and 15(b), it can be seen that the

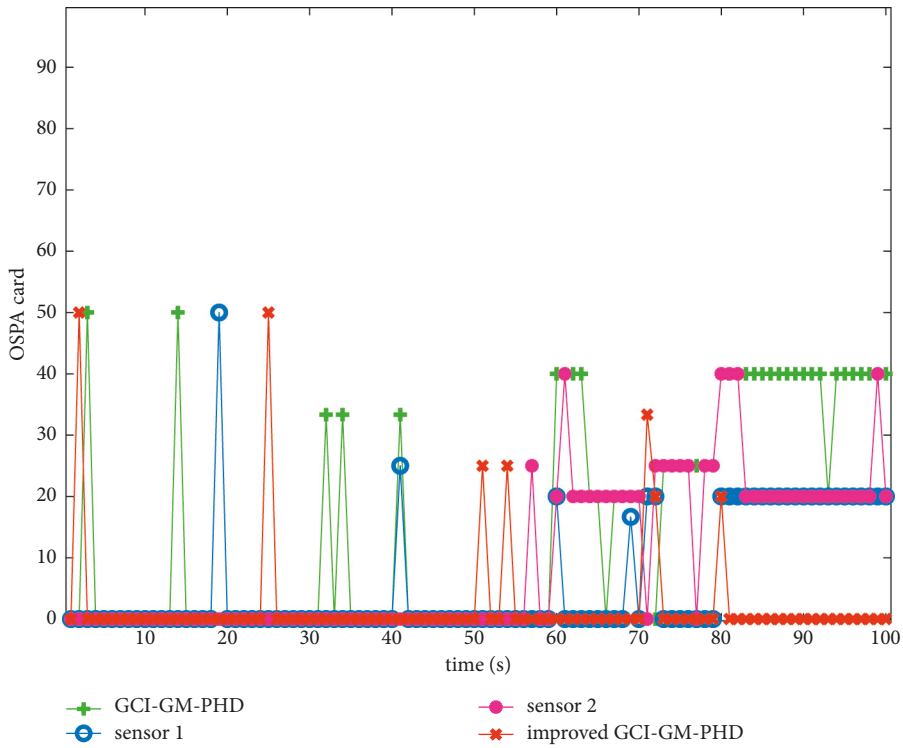

Figure 12: Comparison of cardinalities estimation errors.

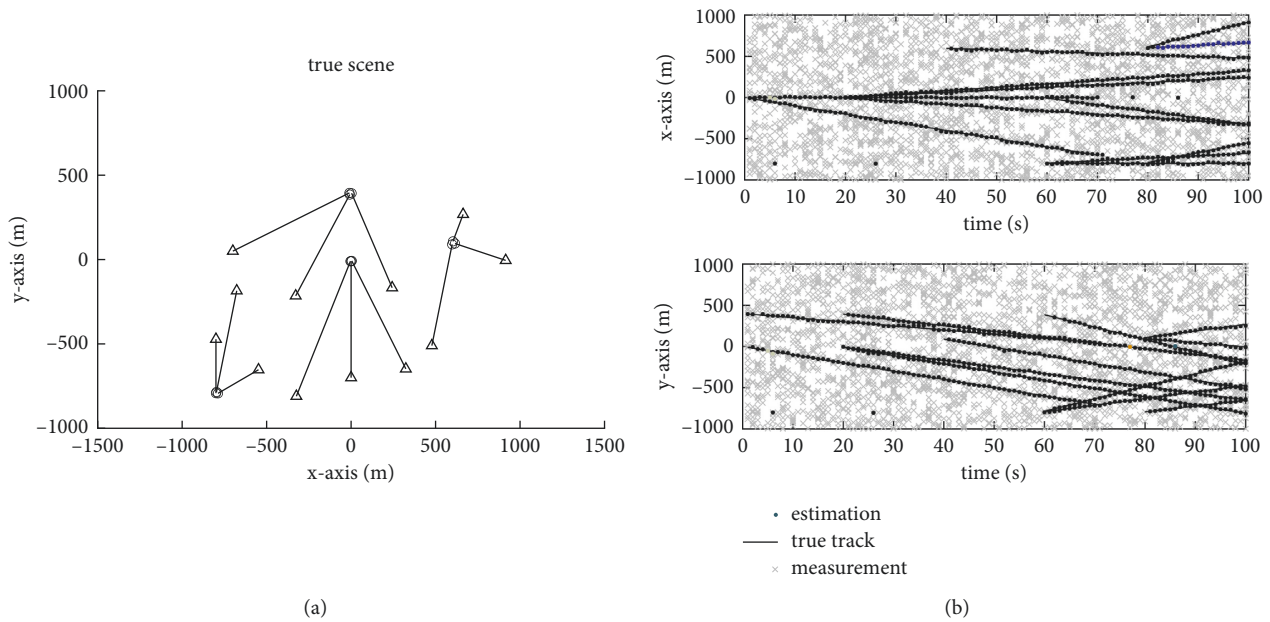

Figure 13: The true trajectory and tracking results of the target when the number of targets increases: (a) true target trajectory; (b) tracking results.

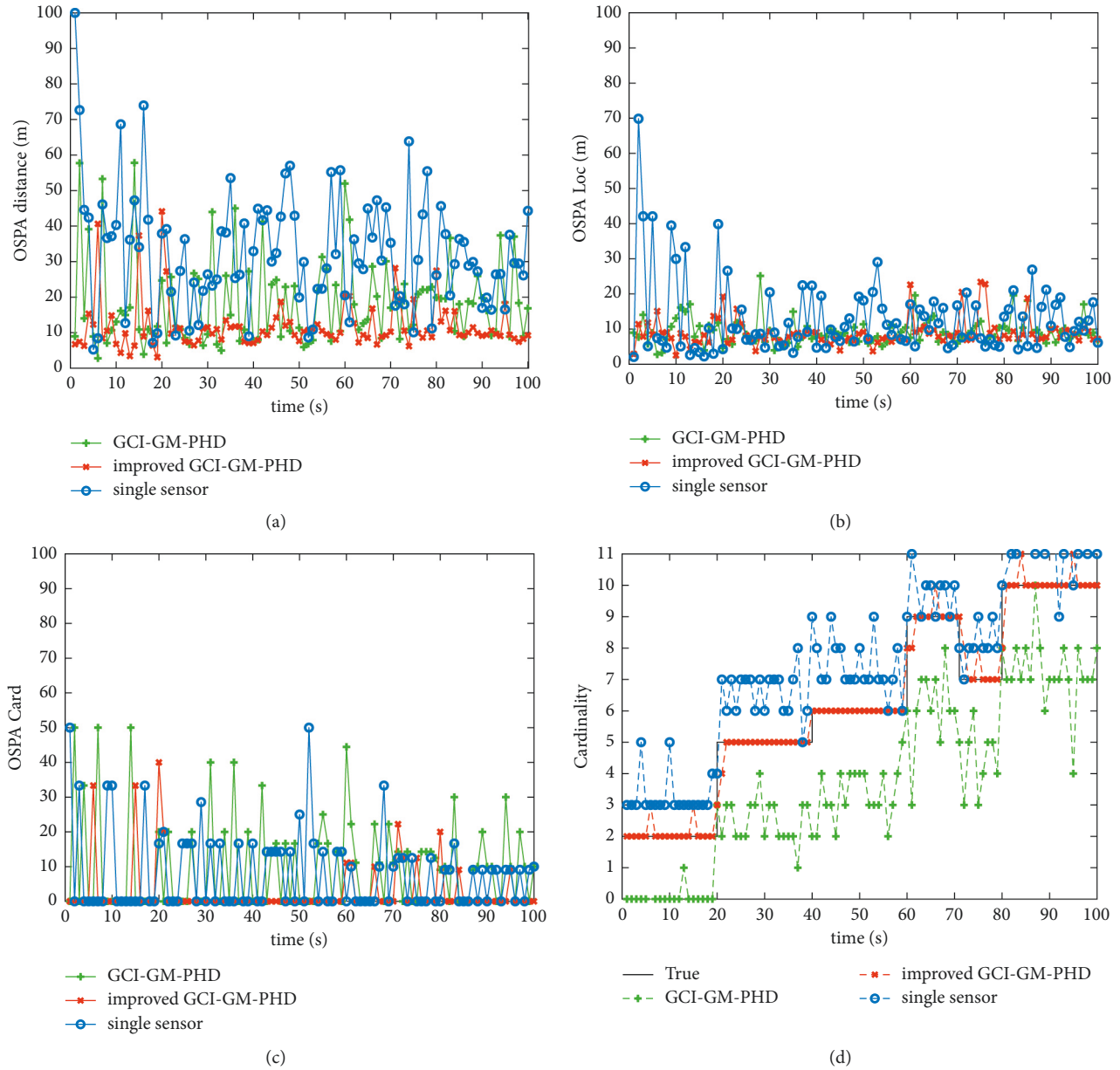

Figure 14: Tracking simulation effect of each algorithm in scene three: (a) OSPA distance comparison; (b) OSPA location comparison; (c) target cardinalities estimation error; (d) estimated cardinalities of targets.

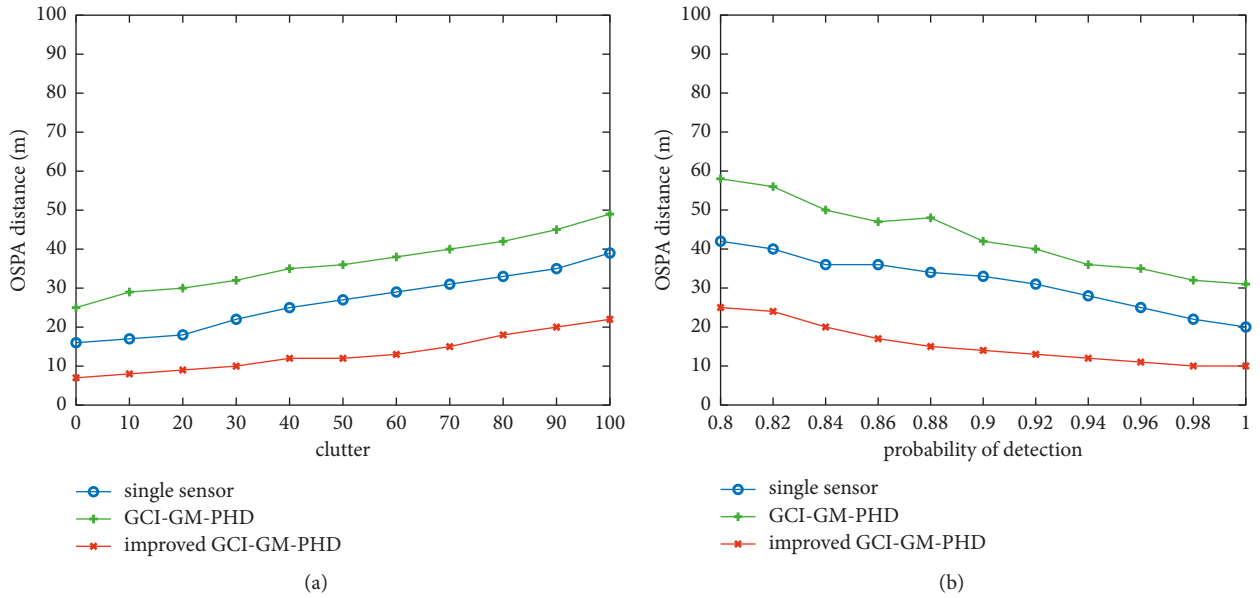

Figure 15: Comparison of OSPA distances with parameter changes: (a) comparison of OSPA distances with different clutter rates; (b) comparison of OSPA distances with different detection probabilities.

improved GCI-GM-PHD algorithm in this paper has the best stability, which indirectly proves the effectiveness and robustness of the algorithm in the multitarget tracking environment.

6. Conclusion

This paper presents an effective and robust method for multitarget and multisensor fusion with limited FoV in distributed environment. Beginning with the analysis of GCI fusion defects of multisensor limited FoV, it puts forward a solution of dividing local Gaussian components into regions and theoretically analyzes the label inconsistency in the process of sensor fusion. What is more, it proposes to find the best match between labels of different sensors by minimizing the label inconsistency index and fuses the Gaussian components corresponding to the matched labels accordingly. The effectiveness of the proposed method is verified by simulation experiments.

In future work, the distributed multisensor fusion method can be applied to more fields. As the air traffic problem mentioned in [60–62], in order to avoid air accidents, this method can be used to install several sensors on the aircraft to avoid collisions, classify the objects, and track them.

Data Availability

The data used to support the findings of the study are available within the article.

Conflicts of Interest

The authors declare that they have no conflicts of interest.

Acknowledgments

This paper was supported by Shaanxi Province Natural Science Basic Research Program, 2022JQ-679.

References

[1] D. Reid, "An algorithm for tracking multiple targets," *IEEE Transactions on Automatic Control*, vol. 24, no. 6, pp. 1202–1211, 1979.

[2] F. Daum, "Multitarget-multisensor tracking: principles and techniques," *IEEE Aerospace and Electronic Systems Magazine*, vol. 11, no. 2, pp. 41–53, 1996.

[3] Y. Bar-Shalom, *Tracking and Data Association*, Academic Press, San Diego, CA, USA, 1988.

[4] Y. Bar-Shalom, T. Kirubarajan, and X. Lin, "Probabilistic dataassociation techniques for target tracking with applicationsto sonar, radar and EO sensors," *IEEE Aerospace and Electronic Systems Magazine*, vol. 20, no. 8, pp. 37–56, 2005.

[5] D. Musicki and R. Evans, "Joint integrated probabilistic dataassociation: jipda," *IEEE Transactions on Aerospace andElectronic Systems*, vol. 40, no. 3, pp. 1093–1099, 2004.

[6] S. S. Blackman, "Multiple hypothesis tracking for multipletarget tracking," *IEEE Aerospace and Electronic Systems Magazine*, vol. 19, no. 1, pp. 5–18, 2004.

[7] R. Mahler, "Multitarget Bayes filtering via first-order multitarget moments," *IEEE Transactions on Aerospace and Electronic Systems*, vol. 39, no. 4, pp. 1152–1178, 2004.

[8] Q. Hu, H. Ji, and Y. Zhang, "A standard PHD filter for joint tracking and classification of maneuvering extended targets using random matrix," *Signal Processing*, vol. 144, no. MAR, pp. 352–363, 2018.

[9] M. R. Leonard and A. M. Zoubir, "Multi-target tracking in distributed sensor networks using particle PHD filters," *Signal Processing*, vol. 159, no. JUN, pp. 130–146, 2019.

[10] Z. Liu, L. Ji, and F. Yang, "Cubature information Gaussian mixture probability hypothesis density approach for multi extended target tracking," *IEEE Access*, no. 99, p. 1, 2019.

[11] P. Feng, W. Wang, and S. Dlay, "Social force model-based MCMC-OCSVM particle PHD filter for multiple human tracking," *IEEE Transactions on Multimedia*, no. 99, p. 1, 2016.

[12] H. Kim, K. Granstrom, and L. Gao, "Joint CKF-PHD filter and map fusion for 5GMulti-cell SLAM," *Proc. of the IEEEInternational Conference on Communications(ICC)*, vol. 324, pp. 1–6, 2020.

[13] Q. Jiang, R. Wang, and C. Zhou, "Modified bayesian group target track initiation algorithm based on algebraic graph theory," *Journal of Electronics and Information Technology*, vol. 43, no. 3, pp. 531–538, 2021.

[14] K. Panta, D. E. Clark, and B. N. Vo, "Data association and track management for the Gaussian mixture probability hypothesis density filter," *IEEE Transactions on Aerospace and Electronic Systems*, vol. 45, no. 3, pp. 1003–1016, 2009.

[15] B. N. Vo, S. Singh, and A. Doucet, "SequentialMonte Carlo methods for multi-target filteringwith random finite sets," *IEEE Transactions on Aerospace and Electronic Systems*, vol. 41, no. 4, pp. 1224–1245, 2005.

[16] D. E. Clark and J. Bell, "Data association for the PHD filter," in *Proceedings of the 2005 International Conference on Intelligent Sensors, Sensor Networks and Information Process-ing*, pp. 217–222, IEEE, Melbourne, Australia, December 2005.

[17] X. Zhou, Y. Tang, and J. Yang, "Penalized Gaussian mixture probability hy-pothesis density tracker with multi-feature fusion," in *Proceedings of the 2014 IEEE International Conference on Robotics and Biomimetics*, pp. 1415–1420, IEEE, Bali, Indonesia, December 2014.

[18] Y. Wang, Z. Jing, and S. Hu, "Data association for PHD filter based on MHT," in *Proceedings of the 2008 11th International Conference on Information Fusion*, pp. 1–8, IEEE, Cologne, Germany, July 2008.

[19] K. Panta, B. N. Vo, and S. Singh, "Novel data association schemes for the probability hypothesis density filterfilter," *IEEE Transactions on Aerospace and Electronic Systems*, vol. 43, no. 2, pp. 556–570, 2007.

[20] K. Panta, D. E. Clark, and B. N. Vo, "Data association and track management for the Gaussian mixture probability hypothesis density filterfilter," *IEEE Trans. Aerosp. Elec-tron. Syst.*vol. 45, no. 3, pp. 1003–1016, 2009.

[21] S. Reuter, B. T. Vo, B. N. Vo, and K. Dietmayer, "The labeled multi-Bernoulli filter," *IEEE Transactions on Signal Processing*, vol. 62, no. 12, pp. 3246–3260, 2014.

[22] B. T. Vo and B. N. Vo, "Labeled random finite sets and multi-object conjugate priorsfinite sets and multi-object conjugate priors," *IEEE Transactions on Signal Processing*, vol. 61, no. 13, pp. 3460–3475, 2013.

[23] B. N. Vo, B. T. Vo, and D. Phung, "Labeled random finite sets and the bayes multi-target tracking filterfinite sets and the bayes multi-target tracking filter," *IEEE Transactions on Signal Processing*, vol. 62, no. 24, pp. 6554–6567, 2014.

[24] K. C. Chang, R. K. Saha, and Y. Bar-Shalom, "On optimal track-to-track fusion," *IEEE Transactions on Aerospace and Electronic Systems*, vol. 33, no. 4, pp. 1271–1276, 1997.

[25] S. Mori, W. H. Barker, C. Y. Chong, and K. C. Chang, "Track association and track fusion with nondeterministic target dynamics," *IEEE Transactions on Aerospace and Electronic Systems*, vol. 38, no. 2, pp. 659–668, 2002.

[26] S. Marano, V. Matta, and P. Willett, "Distributed estimation in large wireless sensor networks via a locally optimum approach," *IEEE Transactions on Signal Processing*, vol. 56, no. 2, pp. 748–756, 2008.

[27] I. D. Schizas, G. B. Giannakis, and Z. Q. Luo, "Distributed estimation using reduced-di- mensionality sensor observations," *IEEE Transactions on Signal Processing*, vol. 55, no. 8, pp. 4284–4299, 2007.

[28] F. S. Cattivelli, C. G. Lopes, and A. H. Sayed, "Diffusion recursive least-squares for dis-tributed estimation over adaptive networks," *IEEE Transactions on Signal Processing*, vol. 56, no. 5, pp. 1865–1877, 2008.

[29] R. Mahler, "Optimal/robust distributed data fusion: a unified approach," *Pro- ceedings of the SPIE Defense Security Symposium*, vol. 20, pp. 128–138, 2018.

[30] D. E. Clark, S. J. Julier, R. Mahler, and B. Ristic, "Robust multi-object sensor fusion with unknown correlations," in *Proceedings of the Sensor Signal Processing Defence*, pp. 1–5, London, UK, September 2010.

[31] A. Dabak, *A Geometry for Detection Theory*, Rice University, Houston, TX, USA, 1992.

[32] G. Battistelli and L. Chisci, "Kullback–Leibler average, consensus on probability densities, and distributed state estimation with guaranteed stability," *Automatica*, vol. 50, no. 3, pp. 707–718, 2014.

[33] M. B. Hurley, "An information theoretic justification for covariance intersection and its generalization," in *Proceedings of the Fifth IEEE International Confer- ence on Information Fusion*, pp. 505–511, Annapolis, MD, USA, July 2002.

[34] G. Battistelli, L. Chisci, C. Fantacci, A. Farina, and R. Mahler, *Distributed Fusion of Multitarget Densities and Consensus PHD/CPHD FIlter 9474*, 2015.

[35] G. Battistelli, L. Chisci, C. Fantacci, A. Farina, and A. Graziano, "Consensus CPHD filter for distributed multitarget trackingfilter for distributed multitarget tracking," *IEEE J. Sel. Top. Signal Process*, vol. 7, no. 3, pp. 508–520, 2013.

[36] M. Üney, D. E. Clark, S. J. Julier, and J. Sel, "Distributed fusion of PHD filters via exponential mixture densitiesfilters via expo- nential mixture densities," *IEEE Journal of Selected Topics in Signal Processing*, vol. 7, no. 3, pp. 521–531, 2013.

[37] W. Yi, M. Jiang, R. Hoseinnezhad, and B. Wang, "Distributed multi-sensor fusion us- ing generalised multi-Bernoulli densities," *IET Radar, Sonar & Navigation*, vol. 11, no. 3, pp. 434–443, 2017.

[38] G. Li, W. Yi, M. Jiang, and L. Kong, "Distributed fusion with PHD filter for multi-tar- get tracking in asynchronous radar system," in *Proceedings of the IEEE Inter- national Radar Conference*, pp. 1434–1439, Seattle, WA, USA, May 2017.

[39] C. Fantacci, B. N. Vo, B. T. Vo, G. Battistelli, and L. Chisci, "Robust fusion for multisen- sor multiobject tracking," *IEEE Signal Processing Letters*, vol. 25, no. 5, pp. 640–644, 2018.

[40] S. Li, W. Yi, R. Hoseinnezhad, G. Battistelli, B. Wang, and L. Kong, "Robust distributed fusion with labeled random finite setsfinite sets," *IEEE Transactions on Signal Processing*, vol. 66, no. 2, pp. 278–293, 2018.

[41] Y. Chai, "Heterogeneous multi-sensor fusion with random finite set multi-object densities," *IEEE Transactions on Signal Processing*, pp. 3399–3414, 2021.

[42] L. Yi and Battistelli, "Distributed multi-sensor fusion of PHD filters with different sensor fields of view," *IEEE Transactions on Signal Processing*, pp. 5204–5218, 2020.

[43] L. Wang and Battistelli, "Multi-agent fusion with different limited fields-of-view," *IEEE Transactions on Signal Processing*, pp. 1560–1575, 2022.

[44] S. Li, G. Battistelli, L. Chisci, W. Yi, B. Wang, and L. Kong, "Computationally efficient multi-agent multi-object tracking

with labeled random finite sets," *IEEE Transactions on Signal Processing*, vol. 67, no. 1, pp. 260–275, 2019.

[45] W. Yi, M. Jiang, S. Li, and B. Wang, "Distributed sensor fusion for RFS density with consideration of limited sensing ability," in *Proceedings of the Twentieth IEEE International Conference on Information Fusion*, pp. 1–7, Xi'an, China, July 2017.

[46] M. R. Balthasar and A. M. Zoubir, "Multi-target tracking in distributed sensor net- works using particle PHD filters," *Signal Processing*, vol. 159, pp. 130–146, 2019.

[47] J. Gan, M. Vasic, and A. Martinoli, "Cooperative multiple dynamic object tracking on moving vehicles based on sequential Monte Carlo probability hypothesis den- sity filter," in *Proceedings of the IEEE International Conference on Intelligent Transportation System*, pp. 2163–2170, Rio de Janeiro, Brazil, November 2016.

[48] G. Battistelli, L. Chisci, and A. Laurenzi, "Random set approach to distributed mul- tivehicle SLAM," *IFAC-PapersOnLine*, vol. 50, no. 1, pp. 2457–2464, 2017.

[49] M. Vasic, D. Mansolino, and A. Martinoli, "A system implementation and evaluation of a cooperative fusion and tracking algorithm based on a Gaussian mixture PHD filter," in *Proceedings of the IEEE International Conference on Intelligent Robots and System*, pp. 4172–4179, Daejeon, Korea (South), 09-14 October 2016.

[50] X. Wang, A. K. Gostar, T. Rathnayake, B. Xu, A. Bab-Hadiashar, and R. Hoseinnezhad, "Centralized multiple-view sensor fusion using labeled multi-Bernoulli filtersfilters," *Signal Processing*, vol. 150, pp. 75–84, 2018.

[51] W. Liu, Y. Chen, and H. Cui, "Multi-sensor tracking with non-overlapping field for the GLMB filter," in *Proceedings of the IEEE International Conference on Con- trol, Automation and Information Sciences*, pp. 197–202, Chiang Mai, Thailand, November 2017.

[52] S. Li, G. Battistelli, L. Chisci, W. Yi, B. Wang, and L. Kong, "Multi-sensor multi-object tracking with different fields-of-view using the LMB filter," in *Proceedings of the Twenty First IEEE International Conference on Information Fusion*, pp. 1201–1208, Cambridge, UK, July 2018.

[53] B. N. Vo and W. K. Ma, "The Gaussian mixture probability hypothesis density filterfilter," *IEEE Transactions on Signal Processing*, vol. 54, no. 11, pp. 4091–4104, 2006.

[54] F. Yang, Y. Wang, Y. Liang, and Q Pan, "A survey of PHD filter based multi-target tracking," *Acta Automatica Sinica*, vol. 39, no. 11, pp. 1944–1956, 2013.

[55] G. Battistelli, L. Chisci, C. Fantacci, A. Farina, and A. Graziano, "Consensus CPHD filter for distributed multi-target tracking," *IEEE Journal of Selected Topics in Signal Processing*, vol. 7, no. 3, pp. 508–520, 2013.

[56] M. Uney, D. E. Clark, and S. J. Julier, "Distributed fusion of PHD filtersvia exponential mixture densities," *IEEE Journal of Selected Topics in Signal Processing*, vol. 7, no. 3, pp. 521–531, 2013.

[57] K. Panta, D. E. Clark, and B.-N. Vo, "Data association and track management for the Gaussian mixture probability hypothesis density filterfilter," *IEEE Transactions on Aerospace and Electronic Systems*, vol. 45, no. 3, pp. 1003–1016, 2009.

[58] S. Q. Li, W. Yi, R. Hoseinnezhad, G. Battistelli, B. L. Wang, and L. J. Kong, "Robust distributed fusion with labeled random finite sets," *IEEE Transactions on Signal Processing*, vol. 66, no. 2, pp. 278–293, 2018.

[59] R. P. Mahler, *Statistical Multisource-Multitarget Information Fusion*, Artech House, Nor-well, MA, USA, 2007.

[60] U. Masud, T. Saeed, H. M. Malaikah, F. U. Islam, and G. Abbas, "Smart assistive system for visually impaired people obstruction avoidance through object detection and classification," *IEEE Access*, vol. 10, pp. 13428–13441, 2022.

[61] U. H. M. Zaman, M. A. Arefin, M. A. Akbar, and M. H. Uddin, "Analytical behavior of soliton solutions to the couple type fractional-order nonlinear evolution equations utilizing a novel technique," *Alexandria Engineering Journal*, vol. 61, no. 12, pp. 11947–11958, 2022.

[62] U. Masud, T. Saeed, F. Akram, H. Malaikah, and A. Akbar, "Unmanned aerial vehicle for laser based biomedical sensor development and examination of device trajectory," *Sensors*, vol. 22, no. 9, p. 3413, 2022.